Catalysis Today 146 (2009) 351–358

Contents lists available at ScienceDirect

Catalysis Today

journal homepage: www.elsevier.com/locate/cattod

# Electrochemical promotion of CO oxidation on Pt/YSZ: The effect of catalyst potential on the induction of highly active stationary and oscillatory states

M.N. Tsampas *, F.M. Sapountzi, C.G. Vayenas

*Department of Chemical Engineering, University of Patras, Greece*

ARTICLE INFO

*Article history:*
Available online 17 July 2009

*Keywords:*
Electrochemical promotion
NEMCA effect
CO oxidation
Pt/YSZ catalyst
Ion spillover

ABSTRACT

We have investigated the kinetics, rate oscillations and electrochemical promotion of CO oxidation on Pt deposited on YSZ using a standard oxygen reference electrode at temperatures 300–400 °C. We have found that electropromotion is small ($\rho < 3$) when the catalyst potential $U_{WR}$, is below 0.4 V and very pronounced ($\rho \sim 9$, $\Lambda \sim 1500$) when $U_{WR}$ exceeds 0.4 V. This sharp transition in the electropromotion behavior is accompanied by an abrupt change in reaction kinetics and in catalyst potential. For fixed temperature this transition, which leads to a highly active electropromoted state, occurs at specific $P_{O_2}^{1/2}/P_{CO}$ ratio and catalyst potential. It is shown via comparison with independent catalyst potential–catalyst work function measurements that the transition corresponds to the onset of extensive $O^{2-}$ spillover from YSZ onto the catalyst surface, and concomitant establishment of an effective double layer at the catalyst–gas interface, which is the cause of the highly active electropromoted state.



## 1. Introduction

Due to its theoretical interest and environmental importance the oxidation of CO on Pt is the most thoroughly studied catalytic system [1–3]. Work on several exciting aspects of CO oxidation, including rate oscillations, has been reviewed several times [1–3].

The electrochemical promotion of catalysis [4–22], which is also known in the literature as the NEMCA effect is a phenomenon where application of a small current or potential on a catalyst which is in contact with a solid electrolyte results to non-Faradaic changes on the catalytic activity and selectivity. In most cases these changes are reversible, as they disappear when the current or potential application is stopped. Two parameters are commonly used to describe the magnitude of electrochemical promotion:

(a) The Faradaic efficiency, $\Lambda$, defined from

$$\Lambda = \frac{\Delta r}{(I/2F)} \tag{1}$$

where $\Delta r$ is the change in the catalytic rate caused by the current or potential application, $I$ is the applied current and $F$ is the Faraday's constant. When $|\Lambda| > 1$, the changes in the catalytic rate are non-Faradaic and the reaction exhibits NEMCA behavior, while pure electrocatalysis is limited to $|\Lambda| \leq 1$.

(b) the rate enhancement ratio, $\rho$, defined from

$$\rho = \frac{r}{r_o} \tag{2}$$

where $r$ is the electrochemically promoted catalytic rate and $r_o$ is the open circuit, unpromoted catalytic rate [4].

The oxidation of CO on polycrystalline Pt films deposited $Y_2O_3$–$ZrO_2$ (YSZ) was one of the first catalytic reactions studied in detailed using solid electrolyte potentiometry (SEP) [23] with emphasis in understanding its oscillatory behavior [23,24]. Furthermore it was one of the three first reactions used to study the effect of electrochemical promotion [25]. This early study [25] was exploratory and did not involve any detailed investigation of the effect of the catalyst potential under electropromotion conditions on the reaction kinetics.

Furthermore this study preceded the establishment of the catalyst potential–catalyst work function relationship in YSZ supported catalyst films [5] and the establishment of the standard oxygen electrode (SOE) scale of solid electrolyte electrochemistry [26–28] and also the development of the $O^{2-}$ spillover mechanism of electrochemical promotion [5]. Thus in the present investigation we have focused on the study of the effect of the catalyst potential in the SOE scale on the kinetics and electropromotion of CO oxidation on Pt/YSZ and for this purpose have used the original "fuel cell" type design (Fig. 1) where the counter and reference

* Corresponding author. Tel.: +30 2610 997860.
*E-mail address:* mihalis@chemeng.upatras.gr (M.N. Tsampas).

0920-5861/$ – see front matter © 2009 Elsevier B.V. All rights reserved.
doi:10.1016/j.cattod.2009.06.007

electrodes are kept in air ($P_{O_2} = 21$ kPa) thus establishing a proper reference $O_2$ electrode which is not the case when using the common single chamber cell design [4].

## 2. Experimental

The Pt catalyst film (2 $cm^2$ superficial area) was deposited using Engelhard Pt A1121 paste as described elsewhere [4], i.e. via application of a thin coating of paste followed by drying and calcination first (3 °C/min) to 450 °C for 1 h and then (2 °C/min) to 850 °C for 2 h [6], on the inside surface of the bottom of a YSZ tube closed flat at one end (Fig. 1). The counter electrode, as well as a small (1 $mm^2$) reference electrode at the edge of the YSZ tube, was deposited on the other side of the YSZ tube, which was exposed to ambient air. For reproducibility reasons two catalyst films, labeled catalyst C1 and C2, were tested.

The Pt surface area $N_G$ (expressed in mol Pt) was estimated using the current interruption technique and the corresponding expression [4]:

$$\Lambda_{max} = \frac{r_{max}/N}{1/\tau_D}; \quad N_G = \frac{r_{max}}{\Lambda_{max}}\tau_D \tag{3}$$

where $r_{max}$ and $\Lambda_{max}$ are the maximum rate and $\Lambda$ values obtained in a galvanostatic (constant current) NEMCA transient and $\tau_D$ is the relaxation time of the rate upon current interruption.

This procedure is more exact that the usual galvanostatic transient technique [4] which is based on measuring the time, $\tau_R$, needed for the rate increase to reach 63% of its steady state value upon current application during galvanostatic rate transients, and using the expression $N_G = (I/2F)\tau_R$, because in the present case of CO oxidation on Pt, the observed galvanostatic transient, upon current imposition were sharp and often complicated by surface transitions, so that $\tau_R$ was not easy to measure with sufficient accuracy.

The thus determined surface areas of the two catalysts tested (labeled C1 and C2, respectively) expressed in mol Pt, were $2.9 \times 10^{-8}$ mol and $1.2 \times 10^{-8}$ mol. These values were used to compute the turnover frequencies (TOFs, i.e. oxygen atoms reacting per surface Pt atom per s) from the measured rate data.

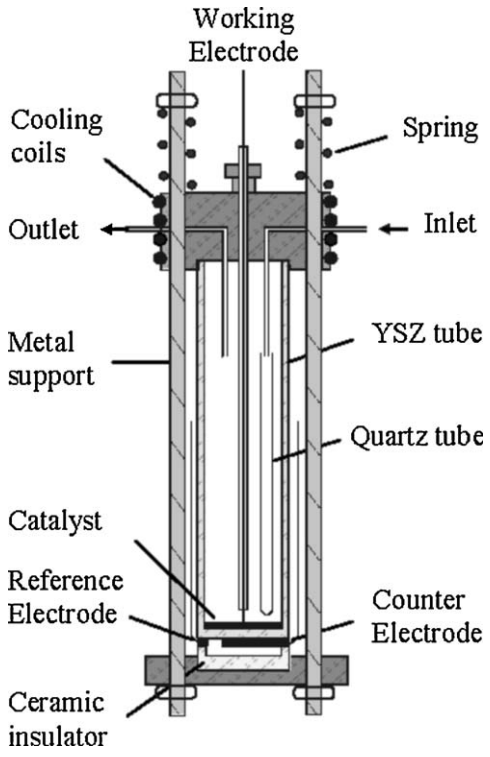


**Fig. 1.** Schematic of the catalytic reactor and of the three electrode arrangement (catalyst, counter and reference).

Reactants were Messer Griesheim-certified standards of 5.02% CO in He and 2.298% and 20.351% $O_2$ in He. They could be further diluted in ultrapure (99.999%) He (Air Liquide). The flow rate in all experiments was 220 $cm^3$/min (STP).

The analysis of the products was carried out by using an infrared CO, $CO_2$ analyzer (FUZI Electric) and a gas chromatograph (SHIMADZU 2014). A galvanostat/potentiostat (AMEL 2053) was used to impose constant currents or potentials. The reaction rate was computed from $r_{CO_2} = Gy_{CO_2}$ where $y_{CO_2}$ is the mol fraction of $CO_2$ in the product stream and $G$ is total molar flowrate (mol/s) which typically changes less than 0.1% in the reactor. The latter was operated quasi-differentially and with maximum electro-promoted conversion of 20%. Note that since this type of reactor has been shown, by measuring its residence time distribution (RTD) to behave as CSTR [4], no error in relating $r_{CO_2}$ with the exit $P_{O_2}$ and $P_{CO}$ values is introduced even at high conversions.

## 3. Results

### 3.1. Open-circuit kinetics and catalyst potential

Fig. 2a and b show the reaction kinetics at 320 °C with respect to $P_{O_2}$ (Fig. 2a) and with respect to $P_{CO}$ (Fig. 2b). The former was varied between 0.1 and 10 kPa, the latter between 0.4 and 2 kPa. The figures also show the corresponding dependence of the catalyst potential $U_{WR}$. One observes that the catalytic rate is positive order (~0.8) with respect to $P_{O_2}$ and negative order (−0.5 to −0.8) with respect to $P_{CO}$. The catalyst potential is between −400 mV and −600 mV, similarly to [23] and increases gradually with increasing $P_{O_2}$. In view of the fact that increasing $U_{WR}$ corresponds to increasing work function $\Phi$ [5,26–28], this shows that adsorbed O behaves, as expected, as an electron acceptor, i.e. it increases the catalyst work function. The effect of $P_{CO}$ on $U_{WR}$ at fixed $P_{O_2}$ is more complex (Fig. 2b) showing that CO behaves either as an electron acceptor or as an electron donor depending on the value of $P_{O_2}$.

It should be noted that, as shown in Fig. 3, and as to be expected from well known oscillatory nature of CO oxidation on Pt [1–3,24], the open-circuit ($I = 0$) catalytic rate was found to practically always exhibit small amplitude self-sustained oscillations with period of the order of a few min, but the amplitude is small (<20% and in most cases <5%), so Fig. 2 presents the average measured rate values. In view of the very large observed electrochemical promotion effects upon current application, including large amplitude rate and potential oscillations, we have not attempted to study these small amplitude rate and $U_{WR}$ oscillations in any detail.

### 3.2. Galvanostatic catalytic transients

Fig. 3a shows the transient effect of positive current application and interruption on the catalytic rate of CO oxidation using catalyst C1. Initially ($t < 0$) the electrical circuit is open and the open-circuit (unpromoted) catalytic rate is $3.32 \times 10^{-8}$ mol/s. At $t = 0$ a positive current ($I = 30$ μA) is applied between the working and counter electrodes and thus $O^{2-}$ are supplied to the catalyst, at the rate $I/2F = 1.55 \times 10^{-11}$ mol/s. This causes a nearly threefold enhancement in the catalytic rate ($\rho = 2.9$). The rate increase, $\Delta r$, is 412 times larger than the rate of $O^{2-}$ supply, thus the Faradaic efficiency $\Lambda$ equals 412. Upon current interruption the catalytic rate (as also the catalyst potential $U_{WR}$) decays to its initial value over a relaxation time period denoted $\tau_D$, of several minutes, which reflects the kinetics of consumption of the backspillover $O^{\delta-}$

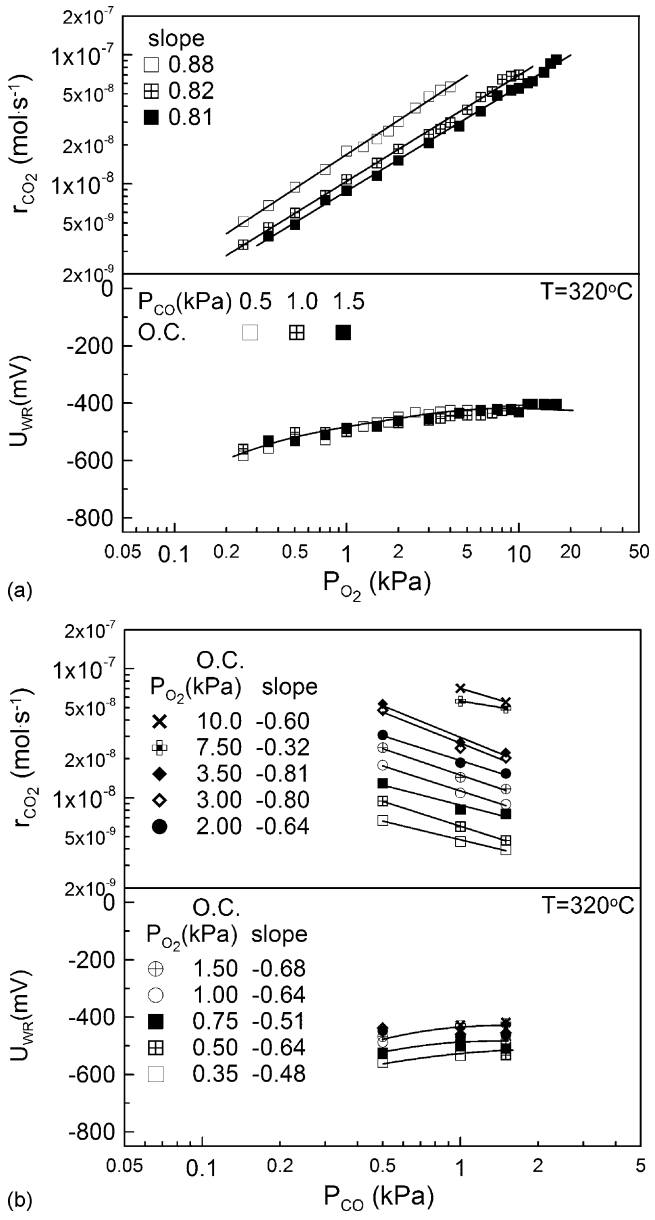


**Fig. 2.** a: Effect of the partial pressure of oxygen on the catalytic rate of CO oxidation on Pt/YSZ under open-circuit conditions (catalyst C1). b: Effect of the partial pressure of CO on the catalytic rate of CO oxidation on Pt/YSZ under open-circuit conditions (catalyst C1).

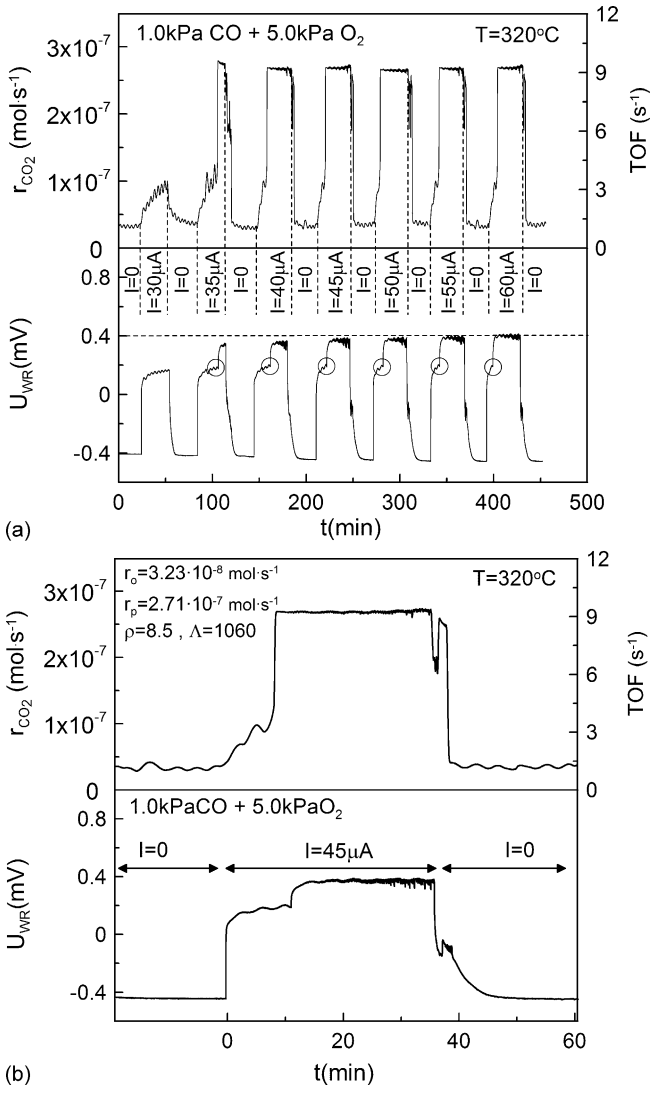


**Fig. 3.** a: Rate and catalyst potential response to step changes in various applied currents during CO oxidation on Pt/YSZ (catalyst C1). b: Rate and catalyst potential response to an applied current of 45 μA (catalyst C1).

species from the catalyst surface [4] and was already used to compute $N_G$ ($2.9 \times 10^{-8}$ mol Pt) as described in Section 2.

While the application of $I = 30$ μA has a modest effect on the catalytic rate (Fig. 3a) as also shown in the same figure application of larger current leads to a modest initial rate increase, followed by an abrupt increase leading to $\rho$ values near 8 (700% rate increase) and $\Lambda$ values of 1000–1200. It is interesting to note the corresponding abrupt changes in the catalyst potential which reaches values very near to +400 mV in the fully electropromoted state. Such a transient is shown in more detail in Fig. 3b. It is interesting to note the peculiar rate and potential response upon current interruption. The spike in $U_{WR}$ always occurs near 0 V.

Fig. 4, obtained with the second catalyst film C2, shows the effect of $P_{O_2}$ on the electrochemical promotion upon positive current application and interruption, at four different temperatures. One observes that increasing $P_{O_2}$ enhances the rate increase and stabilizes the highly active electropromoted state. For intermediate temperatures and intermediate $P_{O_2}$ values, current application leads to large amplitude rate oscillations (Fig. 4b and c) the frequency of which increases with temperature. With this sample (C2) the highly active electropromoted state is reached at potentials near 600 mV. The abrupt appearance of the highly active electropromoted state, which we denote as surface phase transformation in Fig. 5, is accompanied by a pronounced change in reaction kinetics as shown in Fig. 5. The oxidation kinetics now become practically zero order in $P_{O_2}$ (Fig. 5a) and positive order in $P_{CO}$ (Fig. 5b).

### 3.3. Exponential current and catalytic rate dependence on catalyst potential

The steady state effect of potential on the oxidation rate and the current is shown in detail in Fig. 6. One observes that over a wide range of potential the current conforms to the Tafel equation [4], i.e.:

$$\ln(I/I_o) = \alpha_a F\eta/RT = \alpha_a F(U_{WR} - U^o_{WR})/RT \quad (4)$$

with $I_o = 0.25$ μA, $U^o_{WR} = -380$ mV and $\alpha_a = 0.45$. When $U_{WR}$ reaches 200 mV, then the highly active electropromoted state is approached and a new, nearly parallel, line is obtained starting at

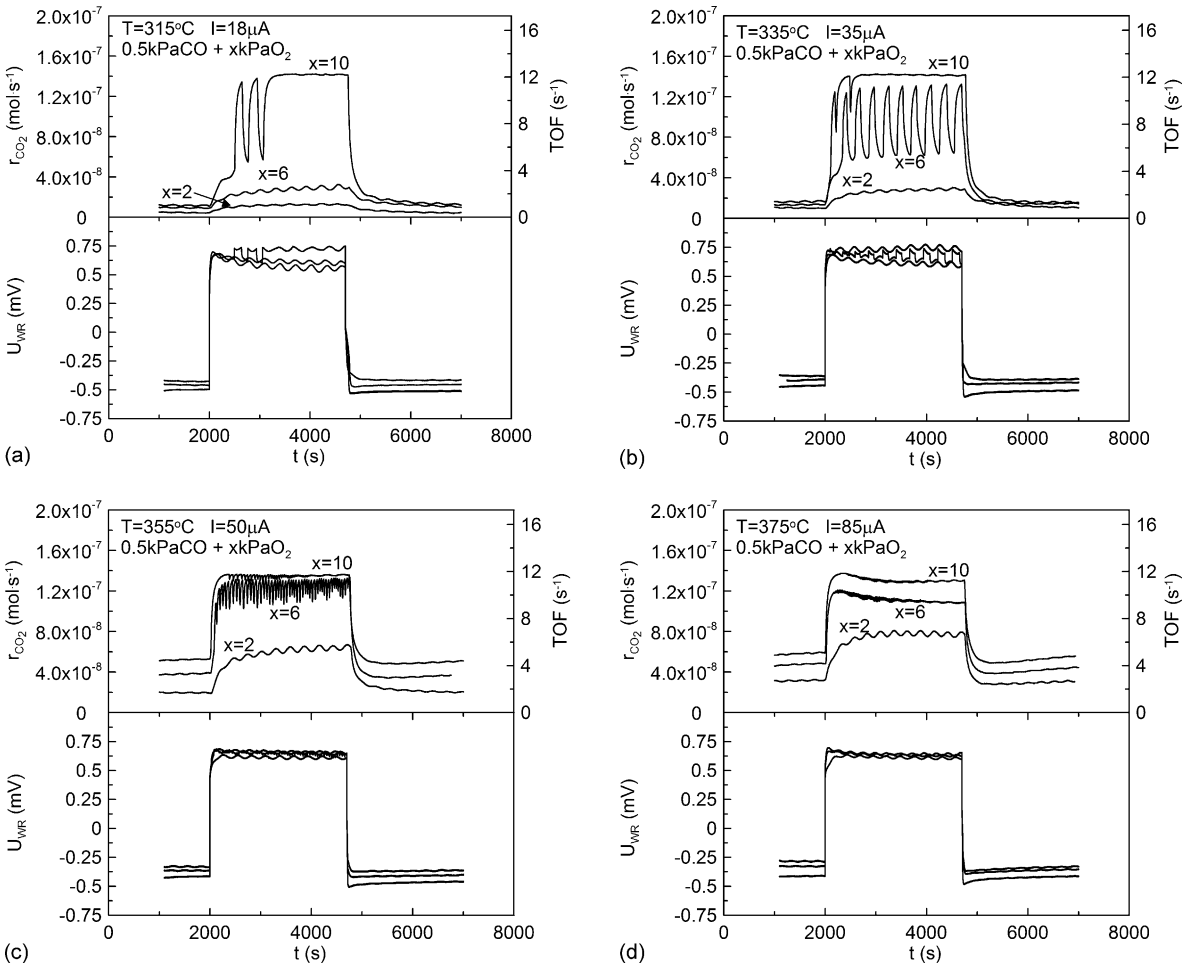


**Fig. 4.** a: Rate and catalyst potential response to step changes in applied current at 315 °C (catalyst C2). b: Rate and catalyst potential response to step changes in applied current at 335 °C (catalyst C2). c: Rate and catalyst potential response to step changes in applied at 355 °C (catalyst C2). d: Rate and catalyst potential response to step changes in applied current at 375 °C (catalyst C2).

$U_{WR}$ = 400 mV. Above this potential the catalytic rate of CO oxidation is practically constant, while at lower potentials it conforms with the classical NEMCA or electrochemical promotion rate equation [4]:

$$\ln(r/r_o) = \alpha_N F\eta/RT = \alpha_a F(U_{WR} - U^*_{WR})/RT \quad (5)$$

with $\alpha_N$ = 0.30 and $U^*_{WR} \approx 0$ mV. The parameter $\alpha_N$ is known as the NEMCA coefficient and is positive for electrophobic reactions, as is the case here. One notes that, as is often the case [4], $\alpha_N$ (~0.30) is smaller than the anodic transfer coefficient $\alpha_a$ (~0.45).

The corresponding effect of potential on $\rho$ and $\Lambda$ is shown in Fig. 7. The former reaches values of 8, the latter reaches values of 1200 in the highly active electropromotion state. As Figs. 8 and 9 show the behavior is qualitatively similar for $P_{CO}$ = 0.5 kPa with the catalyst C2 but in this case larger amplitude rate and potential oscillations occur at lower temperatures and $\Lambda$ reaches values up to 4000. As also shown in Figs. 8 and 9 at temperatures above 355 °C the maximum $\rho$ value decreases gradually from 8 to 2 with a concomitant decrease in $\Lambda$.

An important common feature of both catalysts shown clearly in Figs. 6–9, is that highly active electropromoted state is always obtained for $U_{WR} \geq 0.4$ V. As shown in Fig. 10 which depicts in detail the effect oft he parameter $P^{1/2}_{O_2}/P_{CO}$ on the catalytic rate and potential $U_{WR}$, for fixed applied current the onset of the highly active electropromoted state always occurs at a fixed value of $P^{1/2}_{O_2}/P_{CO}$, which equals 1.8 $kPa^{-1/2}$ for $I$ = 60 μA (Fig. 10a and b) while this critical $P^{1/2}_{O_2}/P_{CO}$ ratio increases up to 4 with decreasing current (Fig. 10c).

## 4. Discussion

The nature of the highly active electropromoted state can be rationalized by comparing the present results with the work function potential data of Pt films deposited on YSZ used to define the absolute potential and standard oxygen electrode scale in solid state electrochemistry at 400 °C [26–28] (Fig. 11 top which is based on Fig. 8b in ref. [26]). This study utilized a Pt catalyst–electrode and both Ag and Au reference electrodes which gave similar results [26]. Thus in Fig. 11 one observes that at $U_{WR}$ = 400 mV the Pt electrode work function, $\Phi_{Pt}$ reaches values above the work function, $\Phi_{o,Pt}$ = 5.5 eV, of clean Pt due to the potential-controlled spillover of $O^{2-}$ from the YSZ support to the catalyst surfaces and in fact stabilizes with increasing $U_{WR}$ to a value near 5.7 eV. One observes in Fig. 11 that the exponential increase in catalytic rate with potential starts near the potential (+100 mV) where the work function of the Pt exceeds that of the YSZ electrolyte (~5.18 eV) which equals that of the reference electrode [26–28]) and continues up to the potential ($U_{WR}$ = 400 mV) where the work function of the Pt electrode approaches its saturation value of 5.7 eV, manifesting the establishment of a dense $O^{2-}$ double layer formed at the catalyst–gas interface (Fig. 12). It therefore follows from Fig. 11 that the highly active electropromoted state

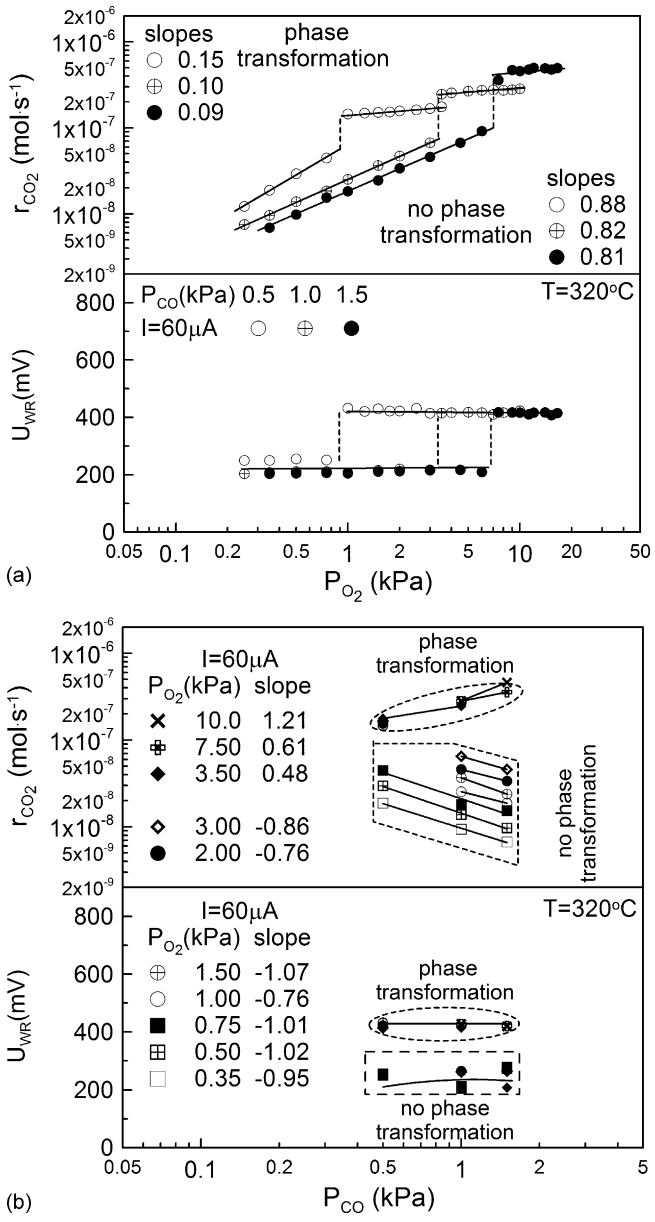


**Fig. 5.** a: Effect of the partial pressure of $O_2$ on the catalytic rate and catalyst potential during application of 60 μA (catalyst C1). b: Effect of the partial pressure of CO on the catalytic rate and catalyst potential during application of 60 μA (catalyst C1).

corresponds exactly to the establishment of this dense effective spillover-formed double layer [4–21].

This double layer has been shown [4,21] to lead to the experimental rate dependence on catalyst potential and work function (Eq. (5)) in the same way that the double layer at the three phase boundaries Pt–YSZ–gas leads to the exponential dependence of the current, i.e. of the electrocatalytic rate, on potential (Tafel Eq. (4)).

The catalyst potential (e.g. $U_{WR}$ = 400 mV) is related to a corresponding value of the surface oxygen activity, $a_O$, via the classical equation of solid electrolyte potentiometry [4]:

$$a_O = (0.21)^{1/2} \exp(FU_{WR}/RT) \quad (6)$$

where $a_O^2$ expresses the partial pressure of $O_2$ which would be in equilibrium with oxygen adsorbed on the catalyst surface if such an equilibrium were established. Thus when $a_O^2 = P_{O_2}$ the adsorbed oxygen is equilibrated with gaseous $O_2$ and when $a_O^2 \ll P_{O_2}$, as,

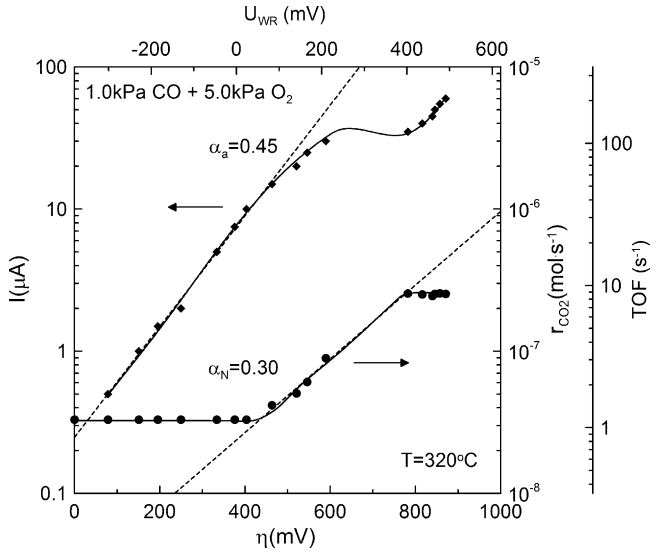


**Fig. 6.** Effect of catalyst potential, $U_{WR}$, and overpotential, $\eta$, on the current and on the catalytic rate of CO oxidation on Pt/YSZ (catalyst C1).

similarly to here, is often the case [4], then the fast catalytic consumption of adsorbed oxygen on the catalyst surface, does not allow equilibrium between gaseous and adsorbed oxygen.

Thus one can also rationalize the observation that the phase transition leading to the electropromoted state occurs at fixed values of $P_{O_2}^{1/2}/P_{CO}$ by considering a steady state mass balance of dissociatively adsorbed oxygen [4]. Thus the coverage, $\theta_O$, of dissociatively adsorbed O, can be computed from:

$$k_{ad}P_{O_2}^{1/2}(1-\theta_O) = k_r P_{CO}\theta_O \quad (7)$$

Assuming, as a first approximation [4], a Langmuir type isotherm, i.e. [4]:

$$\theta_O/(1-\theta_O) = k_O a_O \quad (8)$$

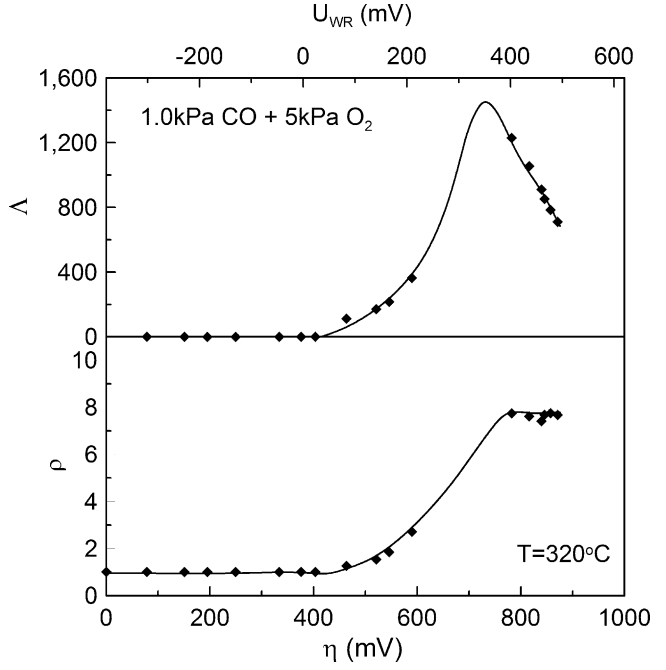


**Fig. 7.** Effect of catalyst potential, $U_{WR}$, and overpotential, $\eta$, on the Faradaic efficiency $\Lambda$ and the rate enhancement ratio $\rho$ (catalyst C1).

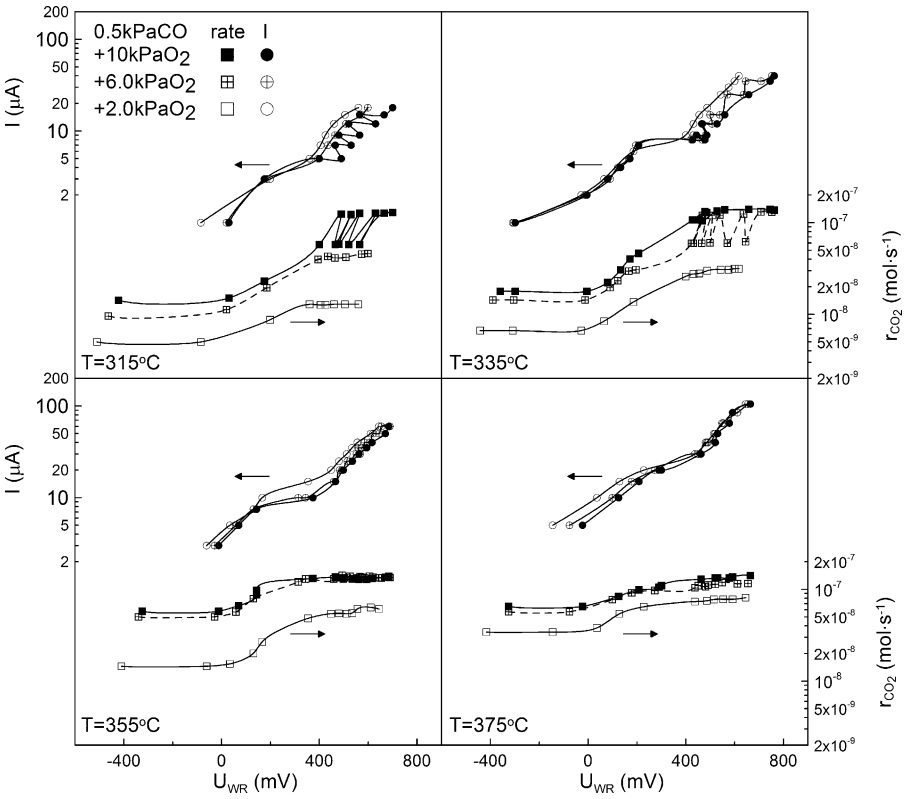


**Fig. 8.** Effect of catalyst potential, $U_{WR}$, on the current and on the catalytic rate of CO oxidation at temperatures 315–375 °C (catalyst C2).

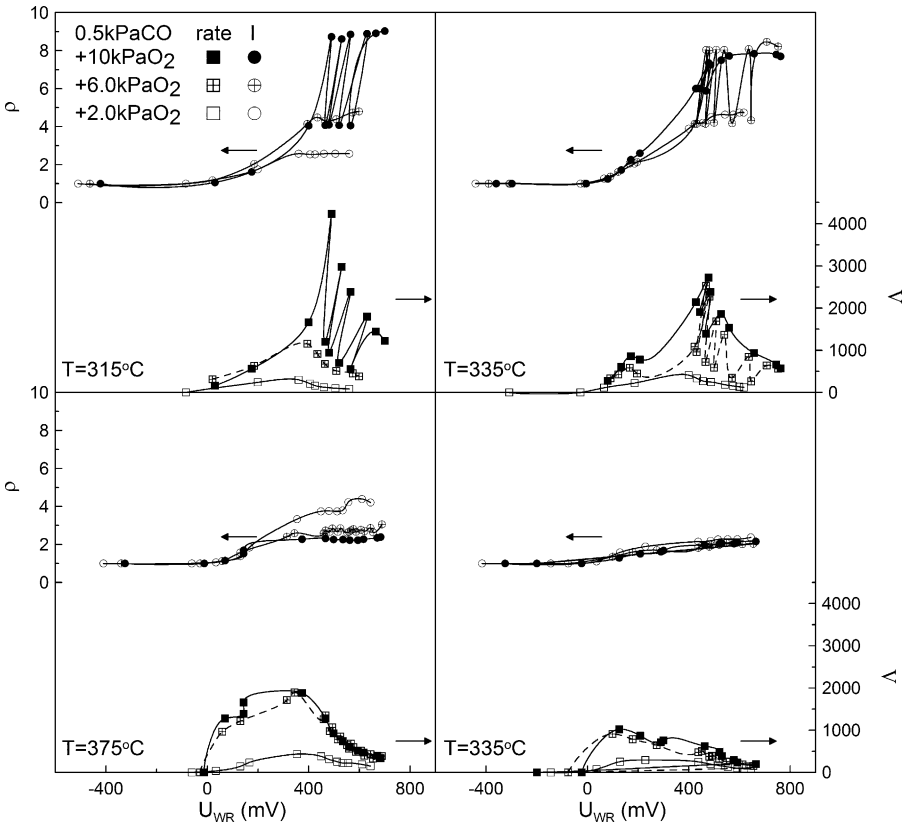


**Fig. 9.** Effect of catalyst potential, $U_{WR}$, on the Faradaic efficiency $\Lambda$ and the rate enhancement ratio $\rho$ at temperatures 315–375 °C (catalyst C2).

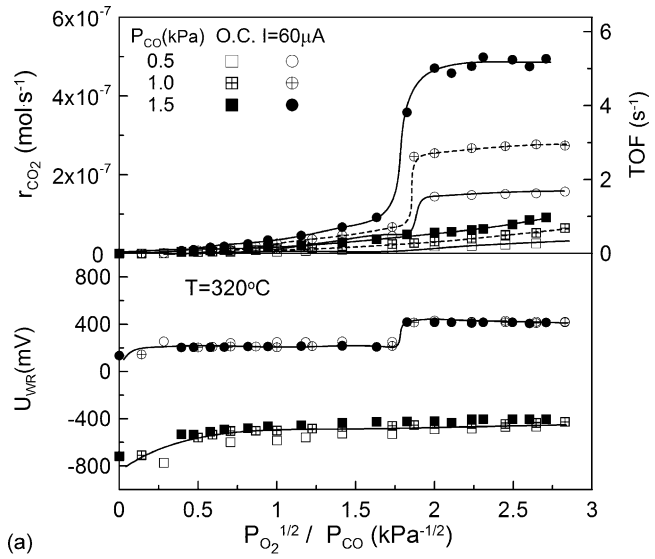


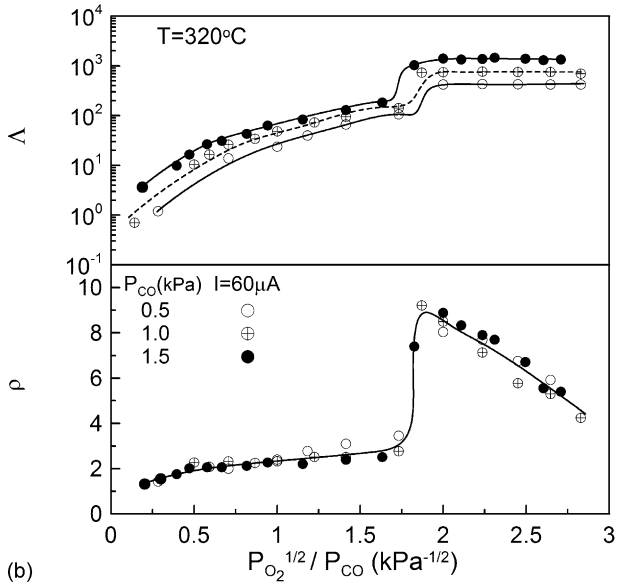


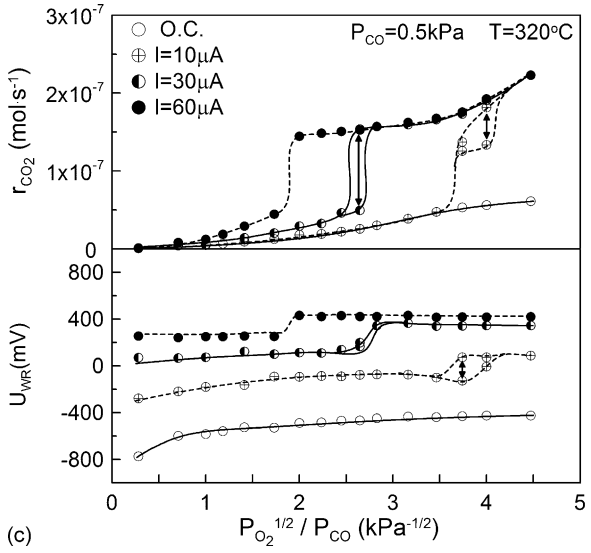


**Fig. 10.** a: Effect of the parameter $P_{O_2}^{1/2}/P_{CO}$ on the rate of $CO_2$ production for three different partial pressures of CO and $I = 60\ \mu A$ (catalyst C1). b: Effect of the parameter $P_{O_2}^{1/2}/P_{CO}$ on the Faradaic efficiency $\Lambda$ and the rate enhancement ratio $\rho$ and $I = 60\ \mu A$ (catalyst C1). c: Effect of applied current and of the parameter $P_{O_2}^{1/2}/P_{CO}$ on the rate of $CO_2$ production and on catalyst potential (catalyst C1).

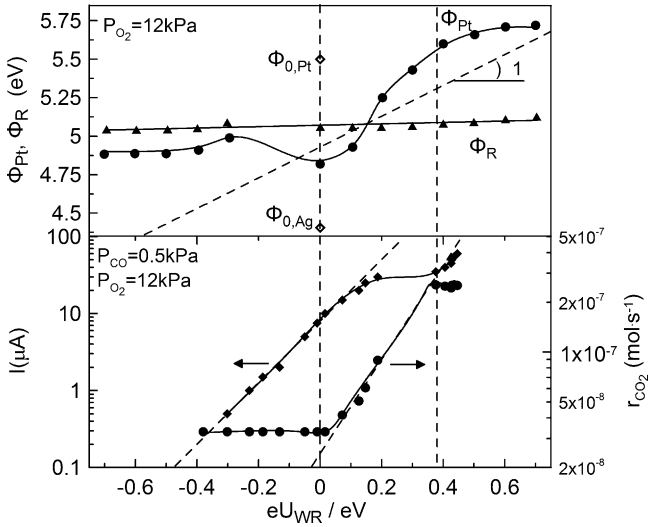


**Fig. 11.** Comparison of Fig. 6 (bottom) with the corresponding effect (top) of catalyst potential $U_{WR}$ on the work function $\Phi_{Pt}$ of similar Pt/YSZ catalyst film measured in situ in ref. [26] (Fig. 8b of ref. [26]) using a Kelvin probe at 400 °C. The top figure also shows the corresponding (negligible) effect of $U_{WR}$ on the work function of the Ag (or Au) reference electrode, which is pinned to the value $5.1 \pm 0.05$ eV corresponding to the absolute potential and Fermi level of the YSZ solid electrolyte [26–28]. Also shown are the values [26], of $\Phi_{o,Pt}$ and $\Phi_{o,Ag}$ of the work function of atomically clean (and thus not anion spillover modified) polycrystalline Pt and Ag films.

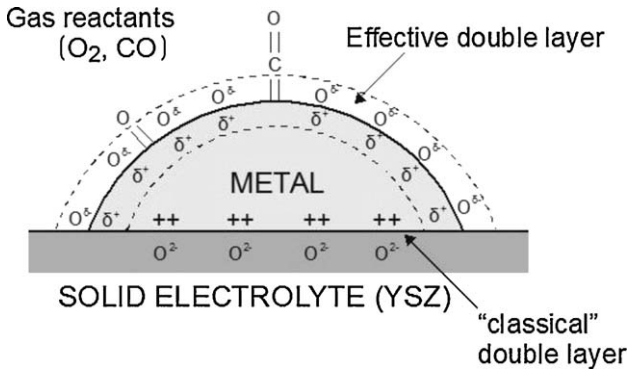


**Fig. 12.** Schematic representation of a the metal catalyst electrode deposited on the YSZ $O^{2-}$ conducting solid electrolyte, showing the location of the metal–electrolyte double layer and of the effective double layer created at the metal/gas interface due to potential-controlled ion migration (spillover) [4] leading to the highly active electropromoted state.

it follows from (7) and (8) that:

$$a_O = (k_{ad}/k_r k_O) P_{O_2}^{1/2}/P_{CO} \quad (9)$$

which rationalizes the observation that ratio $P_{O_2}^{1/2}/P_{CO}$ dictates the critical surface oxygen activity and thus the corresponding via (6) critical catalyst potential value, $U_{WR}$, for the onset of extensive $O^{2-}$ spillover to the catalyst surface and thus the creation of the highly active electropromoted state.

## 5. Conclusions

The electrochemical promotion of the CO oxidation on Pt is pronounced and leads to a highly active electropromoted state ($\rho$ up to 8, $\Lambda$ up to 4000), where the kinetics are positive order in $P_{CO}$ and near zero order in $P_{O_2}$. This highly active electropromoted state corresponds to catalyst potentials above 0.4 V in the SOE scale [26–28] and thus to work functions above 5.6 eV in the absolute potential scale. In this state a dense double layer is established at

the metal–gas interface by the spillover $O^{2-}$ ions and their compensating charge on the metal [4,21]. Although none of these observations taken by itself is new in the solid state electrochemistry absolute potential literature [26–28] or in the electrochemical promotion literature [4], it is probably the first time that these observations are directly combined as in Fig. 11, to rationalize the observed pronounced electrochemical promotion of CO oxidation.

## Acknowledgements

We thank the Apollon B programme of the EU for financial support and our reviewers for some very helpful suggestions.

## References

[1] R. Imbihl, G. Ertl, Chem. Rev. 95 (1995) 697.
[2] V.P. Zhdanov, B. Kasemo, J. Catal. 220 (2003) 478.
[3] K. Arnby, A. Torncrona, B. Anderson, M. Skoglundh, J. Catal. 221 (2004) 252.
[4] C.G. Vayenas, S. Bebelis, C. Pliangos, S. Brosda, D. Tsiplakides, Electrochemical Activation of Catalysis: Promotion Electrochemical Promotion and Metal-Support Interactions, Kluwer Academic/Plenum Publishers, New York, 2001.
[5] C.G. Vayenas, S. Bebelis, S. Ladas, Nature 343 (1990) 625.
[6] M. Stoukides, C.G. Vayenas, J. Catal. 70 (1981) 137.
[7] C.G. Vayenas, S. Bebelis, S. Neophytides, J. Phys. Chem. 92 (1988) 5083.
[8] T.I. Politova, V.A. Sobyanin, V.D. Belyaev, React. Kinet. Catal. Lett. 41 (1990) 321.
[9] N.A. Anastasijevic, H. Baltruschat, J. Heitbaum, Electrochim. Acta 38 (1993) 1067.
[10] S. Bebelis, C.G. Vayenas, J. Catal. 118 (1989) 125.
[11] J. Pritchard, Nature (London) 343 (1990) 592.
[12] R. Lambert, in: A. Wieckowski, E.R. Savinova, C.G. Vayenas (Eds.), Catalysis and Electrocatalysis at Nanoparticle Surfaces, Marcel Dekker, Inc., New York, 2003.
[13] Ch. Kokkofitis, G. Karagiannakis, S. Zisekas, M. Stoukides, J. Catal. 234 (2005) 476.
[14] N. Kotsionopoulos, S. Bebelis, J. Appl. Electrochem. 35 (2005) 1253.
[15] D. Poulidi, A. Thursfield, I.S. Metcalfe, Top. Catal. 44 (3) (2007) 435.
[16] S. Neophytides, D. Tsiplakides, P. Stonehart, M. Jaksic, C.G. Vayenas, Nature (London) 370 (1994) 292.
[17] I.M. Petrushina, V.A. Bandur, F. Cappeln, N.J. Bjerrum, J. Electrochem. Soc. 147 (2000) 3010.
[18] C. Cavalca, G. Larsen, C.G. Vayenas, G. Haller, J. Phys. Chem. 97 (1993) 6115.
[19] X. Li, F. Gaillard, P. Vernoux, Top. Catal. 44 (2007) 391.
[20] G. Pacchioni, F. Illas, S. Neophytides, C.G. Vayenas, J. Phys. Chem. 100 (1996) 16653.
[21] I. Riess, C.G. Vayenas, Solid State Ionics 159 (2003) 313.
[22] A. Jaccoud, C. Falgairette, G. Fóti, Ch. Comninellis, Electrochim. Acta 52 (2007) 7927.
[23] I.V. Yentekakis, C.G. Vayenas, J. Catal. 111 (1998) 170–188.
[24] C.G. Vayenas, J.M. Michaels, Surf. Sci. Lett. 120 (1982) L405–L408.
[25] I.V. Yentekakis, S. Neophytides, C.G. Vayenas, J. Catal. 111 (1998) 152–169.
[26] D. Tsiplakides, C.G. Vayenas, J. Electrochem. Soc. 148 (2001) 189–202.
[27] D. Tsiplakides, C.G. Vayenas, Solid State Ionics 152–153 (2002) 625–639.
[28] D. Tsiplakides, D. Archonta, C.G. Vayenas, Top. Catal. 44 (2007) 469–479.